CHAPTER IV

QM/MM Modeling of the Deglycosylation Reaction in ChiB Catalysis

4.1 Introduction

Chitinase B (ChiB) (EC 3.2.1.14) belonging to a member of glycoside hydrolase (GH) family 18 [1,2] is responsible in the hydrolysis of chitin, a linear insoluble polymer of β-(1,4)-linked *N*-acetylglucosamine (GlcNAc or NAG), which is believed to be the second most abundant polysaccharide on earth after cellulose. This enzyme has received much attention as an attractive target for development of new drugs/inhibitors [3] with either chemotherapeutic potential against fungi, insects and malaria transmission or anti-inflammatory potential against asthma and allergic diseases. Designing such inhibitors with sufficiently high selectivity and affinity requires a detailed understanding of the catalytic mechanism at the atomistic level.

Catalysis in the *S. marcescens* ChiB has been proposed to involve a substrate assisted double-displacement catalysis which leads to the retention of the configuration of the anomeric carbon [4-6]. The overall reaction of ChiB proceeds in two ordered steps i.e., glycosylation and deglycosylation. Two key catalytic residues (i.e., Asp142 and Glu144) have been identified previously by both structural and kinetic studies to play an important

ลิขสิทธิ์มหาวิทยาลัยเชียงใหม่
Copyright© by Chiang Mai University
All rights reserved

role in catalysis of ChiB [4,6,7]. In the glycosylation step, Asp142 assists in formation of an oxazolinium ion intermediate by polarizing the 2-acetamido group of the substrate to increase its nucleophilicity, thereby promoting attack of the carbonyl oxygen (O7) at the anomeric center (C1). Glu144 meanwhile acts as a general acid, encouraging departure of the aglycon leaving group [8] or by means of proton transfer from Glu144. In the deglycosylation step (see Figure 4.1), the oxazolinium intermediate is broken down in a reverse manner of the glycosylation step; Glu144 is believed to act as a general base, promoting the attack of a water molecule at the anomeric center (C1), while Asp142 is thought to facilitate the expulsion of the 2-acetamido group from the anomeric center (C1), yielding the sugar hemiacetal product with overall retention of stereochemistry.

Hybrid or combined QM/MM (quantum mechanics/molecular mechanics) approaches, introduced for enzyme reactions by Warshel and Levitt [9], treat the central reacting system by a quantum chemical method, while representing the remainder of the system by a classical empirical force field model. These techniques have advantage not only to verify the proposed reaction mechanism, but also to elucidate the transition state or the intermediate that beyond achievable by experimental methods. Applications of these techniques to study the enzymatic reaction have increased significantly over the past two decades [10,11]. For the GH enzyme, these QM/MM techniques have increasingly been applied, providing new understanding insight into the hydrolysis of glycosidic bond in various GH enzymes, as evidenced by recent QM/MM studies such as lysozyme [12], endoglucanase [13], β-galactosidase [14], cellulose [15] and Golgi α-mannosidase [16]. For the QM/MM study of hydrolysis mechanism of ChiB, no evidence has been reported so far.

ลิขสิทธิ์มหาวิทยาลัยเชียงใหม่
Copyright© by Chiang Mai University
All rights reserved

Very recently, our groups (J. Jitonnom, V.S. Lee, P. Nimmanpipug, H.A. Rowlands, and A.J. Mulholland, unpublished results) have studied the glycosylation step of *S. marcescens* ChiB by using combined QM/MM method. Here, we aim to continue our previous QM/MM study in order to fully understand the overall reaction of ChiB.

In this work, the hydrolysis of oxazolinium ion intermediate (deglycosylation step) of the *S. marcescens* ChiB was investigated in detail by using hybrid QM/MM calculations. The QM/MM potential energy surface calculated at AM1-CHARMM22 level was carried out to track the possible reaction pathway and to locate and characterize the structures corresponding to the stationary points for the deglycosylation path of *S. marcescens* ChiB. This study provides important insight into the catalytic mechanism of chitin hydrolysis for the delgycosylation reaction catalyzed by *S. marcescens* ChiB at the atomistic level.

4.2 Methods

4.2.1 Model preparation

The starting model of the ChiB-intermediate complex for the deglycosylation step was built on the basis of the X-ray crystallography structures PDB code [6] of 1E6R and 1E6Z for the *S. marcescens* ChiB complexed with the allosamidin inhibitor and with its reaction intermediate, respectively. These two crystal structures were superimposed by using the chain A of 1E6Z as a template to generate the ChiB-intermediate model structure containing a dimeric product (NAG_2 at subsite –1, –2) and a leaving goup of dimeric sugar (NAG_2 at subsite +1, +2). These subsite numbers indicate the sugar binding

ลิขสิทธิ์มหาวิทยาลัยเชียงใหม่
Copyright © by Chiang Mai University
All rights reserved

subsite of NAG_5 (–2 to +3) following the literature [6]. The observed catalytic water molecule and other crystallographic waters were kept. Hydrogen atoms were added using HBUILD module in CHARMM [17] with all residues in their physiological protonation state. The only exception was the acid/base residue (Glu144), which was deprotonated in the second step as proposed by van Aalten et al. [6] while the Asp142 residue remains protonate.

4.2.2 QM/MM molecular dynamics (MD) simulation

In QM/MM MD simulation, the system was partitioned into QM and MM regions. The QM region consisted of the putative oxazolinium ion intermediate, one catalytic water molecule and side-chain groups of Asp142 and Glu144, leading to a total of 46 atoms (Figure 4.1) which were treated with AM1 semi-empirical method [18]. Three bonds crossing the QM/MM boundary were capped with the 'QQ link atoms' (see Figure 4.1). The charge on the QM system was neutral. Other protein (5871), water (1650) and sugar atoms (131) were treated using the modified version of all-atom CHARMM22 MM force field [19]. The simulations used a stochastic boundary approach [20]. The system was solvated by superimposing a 25 Å radius sphere of TIP3P water molecules centered on the anomeric C1 carbon (see Figure 4.1) and equilibrated for 1.6 ns of CHARMM QM/MM MD simulation by a procedure similar to ref. [21]. MD snapshots were chosen for subsequent restrained QM/MM minimization with Adopted Basis Newton-Raphson method until the gradient was < 0.01 kcal/(mol•Å). The resulting minimized structures were selected as the starting points for reaction path

ลิขสิทธิ์มหาวิทยาลัยเชียงใหม่
Copyright© by Chiang Mai University
All rights reserved

calculation. The simulation was carried out with CHARMM version 27b2 [17]. Geometry optimization of the structures was performed at each point until the gradient was < 0.01 kcal/(mol•Å). The energy was then computed by a single point calculation, removing the energy contributions due to reaction coordinate restraints.

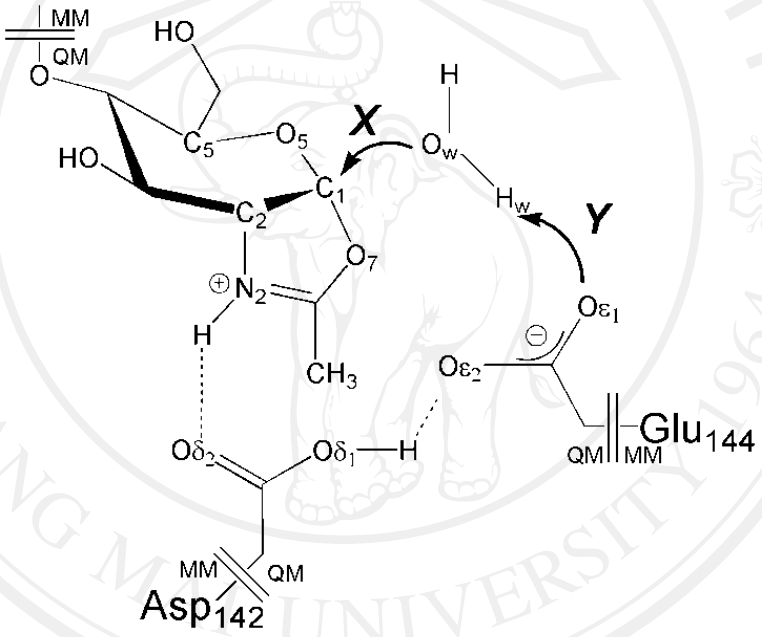

Figure 4.1 QM regions used in this study showing two individual steps for the deglycosylation of *S.marcescens* ChiB (***X*** and ***Y*** represent the nucleophilic attack of catalytic water and proton abstraction, respectively; see text for more details).

ลิขสิทธิ์มหาวิทยาลัยเชียงใหม่
Copyright© by Chiang Mai University
All rights reserved

4.2.3 Reaction path calculation

The two-dimensional (2D) potential energy surface (PES) of a reaction path was determined by adiabatic mapping calculation using CHARMM's RESDistance facility [17]. The reaction described by two discrete coordinates (R_X and R_Y) to represent the two key individual steps of the deglycosylation of *S. marcescens* ChiB (see Figure 4.1), i.e. A proton (H_w) is abstracted from the catalytic water molecule by deprotonated Glu144 (event ***Y***) which described by $R_Y = r[O_w,H_w] - r[O\varepsilon_1,H_w]$, after that such deprotonated water attacks on the anomeric C1 carbon, resulting in a colapse of oxazolinium ion intermediate (event ***X***) which described by $R_X = r[C1,O7] - r[C1,O_w]$. R_X and R_Y were increased in steps of 0.2 Å, respectively, with harmonic restraints of 5000 kcal/(mol•Å^2).

4.3 Results and discussion

4.3.1 Structure of ChiB-intermediate complex

The model of ChiB-intermediate complex is quite stable during the QM/MM MD simulation, demonstrated by the root mean square deviation (RMSD) of about 0.44 ± 0.07 Å, as shown in Figure 4.2. Table 4.1 lists some important geometrical parameters from the X-ray experiment, QM/MM MD simulation and QM/MM minimization. As can be seen, the geometries from our simulation are in good agreement with the X-ray structure. Tyr214 and Asp142 show very stable H-bonds (s.d. < 0.2 Å) during the QM/MM MD simulation (Table 4.1), indicating the importance of these two residues in stabilizing the intermediate (oxazolinium ion). Importantly, the torsion angle (C2–C1–O5–C5) representing the chair conformation of the oxazolinium ion ring is very

ลิขสิทธิ์มหาวิทยาลัยเชียงใหม่
Copyright © by Chiang Mai University
All rights reserved

stable during the simulation which is in excellent agreement with the X-ray experiment (Table 4.1), indicating a good quality of AM1 method to represent the sugar conformation of putative oxazolinium ion ring. Although the simulated distances of C1–O_w and Asp142:Oδ1–Oε2:Glu144 seem to be higher than the experiment, however, these two distances was found to be improved during the restrained QM/MM minimization (see Table 4.1), providing a reasonable starting point for subsequent reaction path calculation.

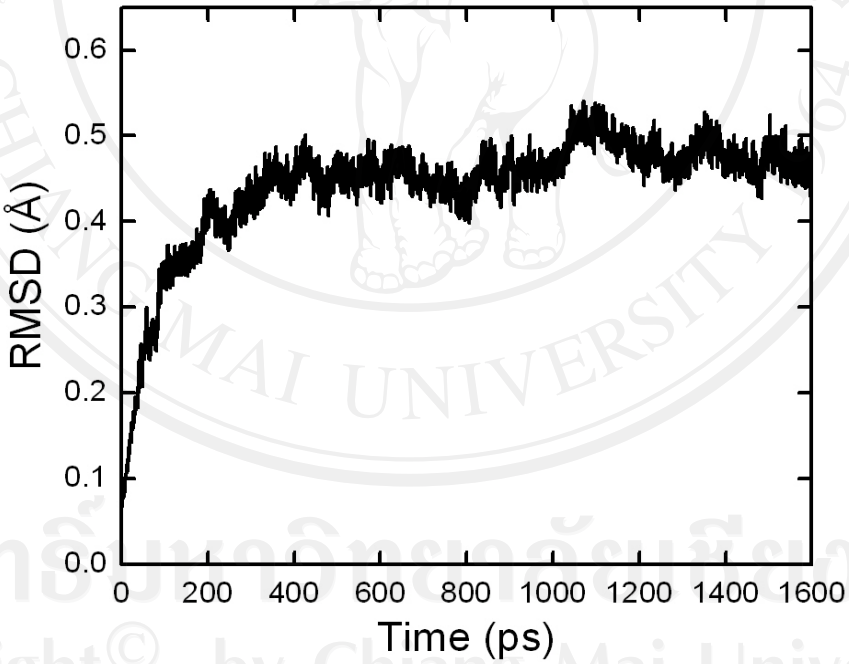

Figure 4.2 Root mean square displacement (RMSD) of the heavy atoms of ChiB-intermediate complex over the time during the 1.6 ns of QM/MM MD simulation.

ลิขสิทธิ์มหาวิทยาลัยเชียงใหม่
Copyright© by Chiang Mai University
All rights reserved

Table 4.1 Some important geometric parameters obtained from experiment (1E6Z), simulation (QM/MM MD) and minimization (QM/MM).

Geometric parameters[a]	experiment	simulation	minimization
C1–O_w	2.75	3.40 ± 0.50	2.76
Glu144:Oε_1–O_w	2.67	2.96 ± 0.51	2.54
Asp142:Oδ_1–Oε_2:Glu144	2.26	3.70 ± 0.55	3.04
N2–Oδ_2:Asp142	2.92	2.88 ± 0.11	2.78
Tyr214: OH–O7	3.05	3.10 ± 0.22	3.12
O_w–C1–O7	152.6	165.8 ± 8.8	146.2
C2–C1–O5–C5	–43.5	–43.5 ± 6.1	–44.2

[a]Atomic numbering correspond to Figure 4.1 whereas other atom types follow the CHARMM format.

4.3.2 Reaction path

Figure 4.3 shows the AM1-CHARMM22 PES describing two key events (see ***X*** and ***Y*** in Figure 4.1) for the nucleophilic attack of oxygen donor (O_w) of catalytic water at the anomeric carbon (C1) acceptor (R_X) and the proton (H_w) abstraction from the water molecule to oxygen atom (Oε_1) of deprotonated Glu144 (R_Y). The stationary points for minima and saddle points located on the PES are also depicted (IM1 : oxazolinium intermediate 1 ; TS1 : transition state 1 ; IM2 : intermediate 2 ; TS2 : transition state 2 ;

ลิขสิทธิ์มหาวิทยาลัยเชียงใหม่
Copyright© by Chiang Mai University
All rights reserved

P : dimer product (NAG_2), see subsite –1, –2). The QM/MM energies on the PES are in kcal/mol.

As indicated in Figure 4.3, the PES clearly shows the presence of two transition states (TS1 and TS2) in the middle of bottom and right-hand of the PES map, respectively, indicating a stepwise mechanism in which the nucleophilic attack would occur as a first step, followed by the proton abstraction. This observation is not expected to happen as its catalytic mechanism has been proposed to occur via only one transition state for the deglycosylation step as well as the glycosylation step [6]. However, our finding here may provide new alternatively possible mechanism for the deglycosylation of *S. marcescens* ChiB. The change of QM/MM energies from IM1→TS1 and IM2→TS2 is 26.8 and 4.0 kcal/mol (Table 4.2), respectively, indicating that the rate-limiting step for the deglycosylation reaction is the nucleophilic attack of catalytic water, showing the calculated barrier of about 27 kcal/mol which is considerably higher than the experimentally determined barriers of 16.1 kcal/mol estimated from the experimental rate constant of 40.9 s^{-1} at 310 K [22] using transition state theory [23]. Although this higher calculated barrier was observed, however, in this study we do not expect to obtain accurate energy barrier and on the other hand we prefer to gain insight into the detailed catalytic mechanism of the deglycosylation of *S. marcescens* ChiB at the atomistic level. Besides, such experimental barrier is estimated based on the overall reaction (i.e., glycosylation and deglycosylation) of *S. marcescens* ChiB [22]. More importantly, no obvious evidence stating the rate-determining step of the ChiB reaction has been reported so far.

ลิขสิทธิ์มหาวิทยาลัยเชียงใหม่
Copyright© by Chiang Mai University
All rights reserved

Additionally, we further analyzed the stabilization energies of the reactive site (i.e., QM region) provided by protein environment (i.e., MM region) along the stationary points relative to that energies in IM1. The result indicates that the influence of protein environment to the stabilization of the reactive site are gradually decreased, as reflected by negative stabilization energies in Table 4.2, providing an evidence that the intermediate (IM1) state is central to catalysis of ChiB.

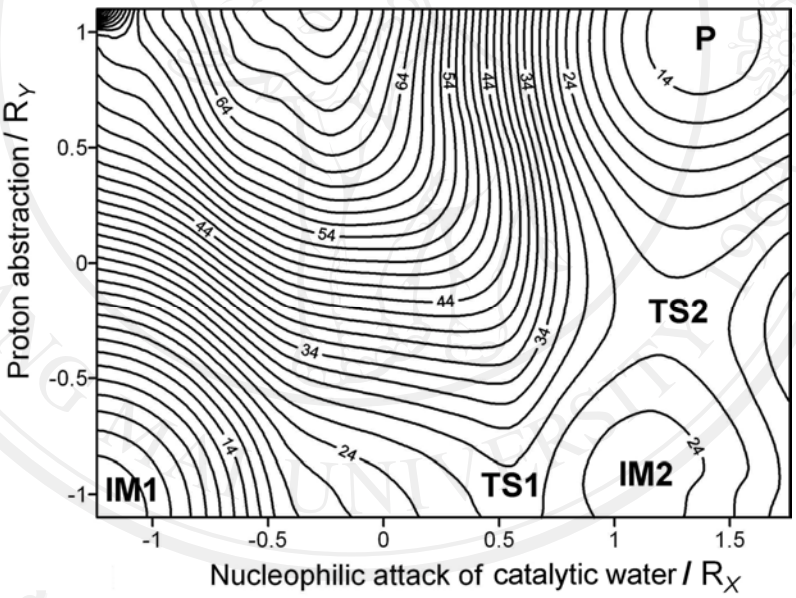

Figure 4.3 AM1-CHARMM22 potential energy surface for the deglycosylation reaction catalyzed by *S. marcescens* ChiB.

ลิขสิทธิ์มหาวิทยาลัยเชียงใหม่
Copyright© by Chiang Mai University
All rights reserved

4.3.3 Geometries along the reaction path

Snapshots of the stationary structures (IM1, TS1, IM2, TS2, and P) and their corresponding geometric parameters along the deglycosylation path of *S. marcescens* ChiB are shown in Figure 4.4 and Table 4.2, respectively. The starting structure of the ground state of ChiB-intermediate (IM1) indicates a suitable position for nucleophilic attack of water molecule as evidenced by distances of C1–O_w (2.73 Å) and Glu144:Oε_1–H_w (2.07 Å) and torsion angle of O_w–C1–O7 (147.7º), which is in good accordance with the X-ray structure shown in Table 4.1. It is also observed that the chair conformation of oxazolinium ring is distorted by about 15º from the X-ray experiment, indicating the importance of relaxed conformation of oxazolinium ring in the beginning of nucleophilic reaction.

In the TS1, the water molecule attacks at the anomeric center (C1) to some extent (Table 4.2) which close enough to break the oxazolinium ring by lengthening the C1–O7 distance for ~1.0 Å from the IM1. At the same time, the chair conformation in the oxazolinium ring is distorted to half-chair, as shown by more planar conformation around the C1–O5 bond (C2–C1–O5–C5 = −11º). Such planarity together with a shortening C1–O5 bond to a partial double bond (1.39 Å at IM1 to 1.32 Å at TS1) indicates the formation of an oxocarbenium-like ion. Note that this half-chair conformation was found to remain until the product state but with increasingly trend of planarity (see C2–C1–O5–C5 in Table 4.2). The Glu144:Oε_1–H_w distance does not change much in this stage, suggesting that no proton abstraction occurs here.

ลิขสิทธิ์มหาวิทยาลัยเชียงใหม่
Copyright © by Chiang Mai University
All rights reserved

In the IM2, as can be seen in Figure 4.4, the water orients itself to be suitable for in-line attack at the anomeric C1 atom as shown by the largest O_w–C1–O7 angle (~160º) and to facilitate the proton abstraction. The proton abstraction initially happens in this stage, as indicated by slightly change of the O_w–H_w (0.98 Å at TS1 to 1.02 Å at IM2) and the Glu144:Oε_1–H_w distance (2.09 Å at TS1 to 1.92 Å at IM2). Meanwhile, the oxygen atom of catalytic water moves closer to the anomeric center (1.96 Å in TS1 to 1.53 Å in IM2) and again the increased C1–O7 distance (2.52 Å in TS1 to 2.69 Å in IM2) is also observed.

In the TS2, the proton abstraction from the water molecule to Glu144 is almost completed in this stage (see Figure 4.4): the distance of the moving proton to the oxygen of Glu144 (Oε_1–H_w) is 1.15 Å, whereas the distance to the water oxygen (O_w–H_w) is 1.35 Å. No significant change for the nucleophilic attack of water molecule. During the proton abstraction, Glu144 is stabilized by the hydrogen atom from Asp142 as indicated by the large decrease in the Hδ_1–Oε2 distance (2.78 Å at IM2 to 2.29 Å at TS2).

In the product (P), the proton abstraction is completed after Glu144 accepts the hydrogen atom (H_w) from deprotonated water, resulting in the expulsion of the 2-acetamido group from the anomeric C1 carbon (2.66 Å at TS2 to 2.79 Å at P). This yields the sugar hemiacetal product with overall retention of stereochemistry. The releasing of dimeric sugar product (NAG at subsite −1, –2, as shown in Figure 4.4) may be indicated by the elongation of H-bond distance of HN2–Oδ_2:Asp142 from 2.13 Å to 2.21 Å (see Table 4.1).

ลิขสิทธิ์มหาวิทยาลัยเชียงใหม่
Copyright© by Chiang Mai University
All rights reserved

Table 4.2 Relevant geometric parameters[a] and energies (in kcal/mol) (i.e., QM/MM and stabilization[b]) of the different stationary structures on the potential energy surface calculated at AM1-CHARMM22 level.

	IM1	TS1	IM2	TS2	P
C1–O_w	2.73	1.96	1.53	1.50	1.43
C1–O7	1.49	2.52	2.69	2.66	2.79
C1–O5	1.39	1.32	1.38	1.39	1.41
O_w–H_w	0.97	0.98	1.02	1.15	2.00
Glu144:Oε_1–H_w	2.07(2.56)[c]	2.09	1.92	1.35	1.00
Asp142:Hδ_1–Oε_2:Glu144	2.70(3.64)[c]	2.82	2.78	2.29	2.48
HN2–Oδ_2:Asp142	2.09(2.83)[c]	2.13	2.13	2.13	2.21
O_w–C1–O7	147.7	150.8	159.1	156.6	151.8
C2–C1–O5–C5	–27.8	–11.1	5.1	1.6	0.4
QM/MM energies	0	26.8	22.7	26.7	12.3
Stabilization energies	0	–22.6	–27.1	–48.9	–71.4

[a] Distances are given in angstroms; angles (i.e., angle and torsion) are given in degrees.

[b] Stabilization energies are the energy difference between full QM/MM system and only QM atoms relative to that of IM1.

[c] Heavy atom distance.

ลิขสิทธิ์มหาวิทยาลัยเชียงใหม่
Copyright© by Chiang Mai University
All rights reserved

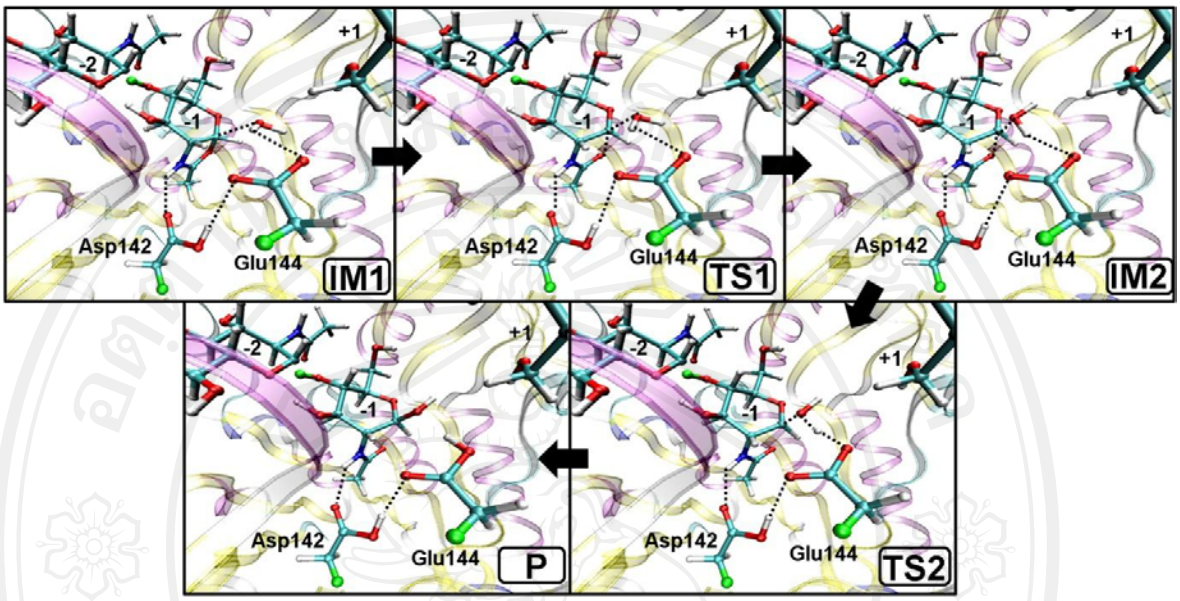

Figure 4.4 Snapshots of the stationary structures along the deglycosylation path of *S. marcescens* ChiB.

4.4 Conclusions

In this study, the deglycosylation step of chitin hydrolysis catalyzed by *S. marcescens* ChiB was investigated for the first time by hybrid QM/MM calculation based on the available crystal structure of ChiB. The QM/MM PES calculated at AM1-CHARMM22 level was carried out using adiabatic mapping to track the possible reaction pathway and to locate and characterize the structures corresponding to the stationary points. The PES shows the presence of two transition states (TS1 and TS2), indicating that the deglycosylation path follows the stepwise mechanism in which the nucleophilic attack of oxygen donor (O_w) of catalytic water at the anomeric carbon (C1) acceptor (R_X) would occur as a first step, followed by the proton (H_w) abstraction from

ลิขสิทธิ์มหาวิทยาลัยเชียงใหม่
Copyright© by Chiang Mai University
All rights reserved

the water molecule to oxygen atom ($O\varepsilon_1$) of deprotonated Glu144 (R_Y). Our results differ from the current knowledge which is believed that the deglycosylation should occur via a single transition state as well as the glycosylaton. However, our finding provides important evidence in that more than one transition state could happen in the deglycosylation of *S. marcescens* ChiB, providing new insight into the catalytic mechanism of ChiB. The calculated barrier for the TS1 and TS2 are 26.8 and 4.0 kcal/mol, suggesting that the nucleophilic attack of water molecule is the rate-limiting step for the deglycosylation. In addition, we also capture the oxocarbenium-like character in the TS1 which is in agreement with the oxocarbenium-like TS observed in the glycosylation step of *S. marcescens* ChiB (see Chapter III). Such oxocarbenium-like ion character, as suggested by our QM/MM studies, is likely to occur in both glycosylation and deglycosylation for the ChiB, supporting the recent finding by Liu et al. [15] in that the formation of oxocarbenium ion transition is a major charateristics for the hydrolysis of β-glycosidic linkage.

References

(1) Henrissat, B. *Biochem. J* **1991**, *280 (Pt 2)*, 309-16.

(2) Davies, G.; Henrissat, B. *Structure* **1995**, *3*, 853-9.

(3) Andersen, O. A.; Dixon, M. J.; Eggleston, I. M.; van Aalten, D. M. F. *Nat. Prod. Rep.* **2005**, *22*, 563-579.

(4) Synstad, B.; Gaseidnes, S.; van Aalten, D. M. F.; Vriend, G.; Nielsen, J. E.; Eijsink, V. G. H. *Eur. J. Biochem.* **2004**, *271*, 253-262.

ลิขสิทธิ์มหาวิทยาลัยเชียงใหม่
Copyright© by Chiang Mai University
All rights reserved

(5) Tews, I.; Terwisscha van Scheltinga, A. C.; Perrakis, A.; Wilson, K. S.; Dijkstra, B. W. *J. Am. Chem. Soc.* **1997**, *119*, 7954-7959.

(6) Van Aalten, D. M. F.; Komander, D.; Synstad, B.; Gaseidnes, S.; Peter, M. G.; Eijsink, V. G. H. *Proc. Natl. Acad. Sci. U.S.A.* **2001**, *98*, 8979-8984.

(7) Vaaje-Kolstad, G.; Houston, D. R.; Rao, F. V.; Peter, M. G.; Synstad, B.; van Aalten, D. M.; Eijsink, V. G. *Biochim. Biophys. Acta* **2004**, *1696*, 103-11.

(8) Cetinbas, N.; Macauley, M. S.; Stubbs, K. A.; Drapala, R.; Vocadlo, D. J. *Biochemistry* **2006**, *45*, 3835-44.

(9) Warshel, A.; Levitt, M. *J. Mol. Biol.* **1976**, *103*, 227-49.

(10) Ranaghan, K. E.; Mulholland, A. J. *Int. Rev. Phys. Chem.* **2010**, *29*, 65 - 133.

(11) Senn Hans, M.; Thiel, W. *Angew. Chem. Int. Ed.* **2009**, *48*, 1198-229.

(12) Bowman, A. L.; Grant, I. M.; Mulholland, A. J. *Chem. Commun.* **2008**, 4425-4427.

(13) Petersen, L.; Ardevol, A.; Rovira, C.; Reilly, P. J. *J. Phys. Chem. B* **2009**, *113*, 7331-7339.

(14) Bras, N. F.; Fernandes, P. A.; Ramos, M. J. *J. Chem. Theory Comput.* **2010**, *6*, 421-433.

(15) Liu, J.; Wang, X.; Xu, D. *J. Phys. Chem. B* **2010**, *114*, 1462-1470.

(16) Petersen, L.; Ardevol, A.; Rovira, C.; Reilly, P. J. *J. Am. Chem. Soc.* **2010**, *132*, 8291-8300.

(17) Brooks, B. R.; Bruccoleri, R. E.; Olafson, B. D.; States, D. J.; Swaminathan, S.; Karplus, M. *J. Comp. Chem.* **1983**, *4*, 187-217.

ลิขสิทธิ์มหาวิทยาลัยเชียงใหม่
Copyright© by Chiang Mai University
All rights reserved

(18) Dewar, M. J. S.; Zoebisch, E. G.; Healy, E. F.; Stewart, J. J. P. *J. Am. Chem. Soc.* **1985**, *107*, 3902-9.

(19) MacKerell, A. D., Jr.; Bashford, D.; Bellott, M.; Dunbrack, R. L.; Evanseck, J. D.; Field, M. J.; Fischer, S.; Gao, J.; Guo, H.; Ha, S.; Joseph-McCarthy, D.; Kuchnir, L.; Kuczera, K.; Lau, F. T. K.; Mattos, C.; Michnick, S.; Ngo, T.; Nguyen, D. T.; Prodhom, B.; Reiher, W. E., III; Roux, B.; Schlenkrich, M.; Smith, J. C.; Stote, R.; Straub, J.; Watanabe, M.; Wiorkiewicz-Kuczera, J.; Yin, D.; Karplus, M. *J. Phys. Chem. B* **1998**, *102*, 3586-3616.

(20) Brooks III, C. L.; Karplus, M. *J. Chem. Phys.* **1983**, *79*, 6312-6325.

(21) Lodola, A.; Mor, M.; Hermann, J. C.; Tarzia, G.; Piomelli, D.; Mulholland, A. J. *Chem. Commun.* **2005**, 4399-4401.

(22) Krokeide, I.-M.; Synstad, B.; Gaseidnes, S.; Horn, S. J.; Eijsink, V. G. H.; Sorlie, M. *Anal. Biochem.* **2007**, *363*, 128-134.

(23) Garcia-Viloca, M.; Gao, J.; Karplus, M.; Truhlar, D. G. *Science* **2004**, *303*, 186-195.

ลิขสิทธิ์มหาวิทยาลัยเชียงใหม่
Copyright© by Chiang Mai University
All rights reserved